

Simultaneous control of ferromagnetism and ferroelasticity by oxygen octahedral backbone stretching

Genhao Liang(梁根豪), Hui Cao(曹慧), Long Cheng(成龙), Junkun Zha(查君坤), Mingrui Bao(保明睿), Fei Ye(叶飞), Hua Zhou(周华), Aidi Zhao(赵爱迪), and Xiaofang Zhai(翟晓芳)

Citation: Chin. Phys. B, 2024, 33 (**9**): 097101. DOI: 10.1088/1674-1056/ad553c
Journal homepage: http://cpb.iphy.ac.cn; http://iopscience.iop.org/cpb

What follows is a list of articles you may be interested in

High-temperature ferromagnetism and strong π-conjugation feature in two-dimensional manganese tetranitride

Ming Yan(闫明), Zhi-Yuan Xie(谢志远), and Miao Gao(高淼)
Chin. Phys. B, 2023, 32 (**3**): 037104. DOI: 10.1088/1674-1056/acae7b

Prediction of one-dimensional CrN nanostructure as a promising ferromagnetic half-metal

Wenyu Xiang(相文雨), Yaping Wang(王亚萍), Weixiao Ji(纪维霄), Wenjie Hou(侯文杰),Shengshi Li(李胜世), and Peiji Wang(王培吉)
Chin. Phys. B, 2023, 32 (**3**): 037103. DOI: 10.1088/1674-1056/acb200

Mottness, phase string, and high-T_c superconductivity

Jing-Yu Zhao(赵靖宇) and Zheng-Yu Weng(翁征宇)
Chin. Phys. B, 2022, 31 (**8**): 087104. DOI: 10.1088/1674-1056/ac7a14

Magnetic and electronic properties of two-dimensional metal-organic frameworks $TM_3(C_2NH)_{12}$

Zhen Feng(冯振), Yi Li(李依), Yaqiang Ma(马亚强), Yipeng An(安义鹏), and Xianqi Dai(戴宪起)
Chin. Phys. B, 2021, 30 (**9**): 097102. DOI: 10.1088/1674-1056/ac0cdb

Point-contact spectroscopy on antiferromagnetic Kondo semiconductors CeT_2Al_{10} (T=Ru and Os)

Jie Li(李洁), Li-Qiang Che(车利强), Tian Le(乐天), Jia-Hao Zhang(张佳浩), Pei-Jie Sun(孙培杰), Toshiro Takabatake, Xin Lu(路欣)
Chin. Phys. B, 2020, 29 (**7**): 077103. DOI: 10.1088/1674-1056/ab8dab

---

RAPID COMMUNICATION

Simultaneous control of ferromagnetism and ferroelasticity by oxygen octahedral backbone stretching

Genhao Liang(梁根豪)[1,2,†], Hui Cao(曹慧)[3,†], Long Cheng(成龙)[2,†,‡], Junkun Zha(查君坤)[1,2], Mingrui Bao(保明睿)[2], Fei Ye(叶飞)[2], Hua Zhou(周华)[4], Aidi Zhao(赵爱迪)[2], and Xiaofang Zhai(翟晓芳)[2,§]

[1] *Department of Physics, University of Science and Technology of China, Hefei* 230026, *China*
[2] *School of Physical Science and Technology, ShanghaiTech University, Shanghai* 201210, *China*
[3] *Materials Science Division, Argonne National Laboratory, Lemont, IL* 60439, *USA*
[4] *X-ray Science Division, Advanced Photon Source, Argonne National Laboratory, Lemont, IL* 60439, *USA*

(Received 24 May 2024; revised manuscript received 4 June 2024; accepted manuscript online 7 June 2024)

Coexistence of ferromagnetism and ferroelasticity in a single material is an intriguing phenomenon, but has been rarely found. Here we studied both the ferromagnetism and ferroelasticity in a group of $LaCoO_3$ films with systematically tuned atomic structures. We found that all films exhibit ferroelastic domains with four-fold symmetry and the larger domain size (higher elasticity) is always accompanied by stronger ferromagnetism. We performed synchrotron x-ray diffraction studies to investigate the backbone structure of the CoO_6 octahedra, and found that both the ferromagnetism and the elasticity are simultaneously enhanced when the in-plane Co–O–Co bond angles are straightened. Therefore the study demonstrates the inextricable correlation between the ferromagnetism and ferroelasticity mediated through the octahedral backbone structure, which may open up new possibilities to develop multifunctional materials.

Keywords: perovskite oxide film, ferromagnetism, ferroelasticity, twin domain

PACS: 71.28.+d, 71.70.Ch, 75.25.–j, 75.47.Lx **DOI:** 10.1088/1674-1056/ad553c

1. Introduction

Complex oxides exhibit many multifunctional properties due to the intricate coupling between the electron, lattice, spin and orbital degrees of freedom, which potentially can be applied in many circumstances, such as energy conversion, data storage, sensor and so on.[1–6] Although the electronic and magnetic properties have been explored for decades in complex oxides, the mechanical properties have been paid much less attention. Recently, there are growing interests in utilizing mechanical interactions to modulate or control the electronic properties.[7–10] Similarly, it is also possible to utilize the mechanical force to manipulate magnetic properties. Previously, typical examples are the piezomagnetic or magnetostrictive materials,[11,12] magnetic thin films integrated on flexible substrates,[13,14] single-phase multiferroic materials or artificially constructed multiferroic composites with magneto–electric–elastic coupling (e.g., $BiFeO_3$,[15] $CaBaCo_4O_7$,[16] $BaTiO_3$–$CoFe_2O_4$,[17] etc.). However, the class of ferromagnetic–ferroelastic coupled multiferroic materials, which also holds great potentials in the magneto-mechanical applications, is rarely explored. Thus new approaches are highly needed for developing such multiferroic materials.

$LaCoO_3$ belongs to the complex oxide family with a perovskite structure that has renewed interest over the last few decades. Bulk $LaCoO_3$ with a filled Co t_{2g}^6 band is diamagnetic at low temperatures and weakly paramagnetic at high temperatures.[18] When tensile-strained by a substrate, the epitaxial $LaCoO_3$ film exhibits a strong ferromagnetic ground state with a Curie temperature as high as 90 K.[19–25] Furthermore, the $LaCoO_3$ films have also been known to exhibit ferroelasticity featured with the formation of stress-induced twin domains.[26–28] The origin of these unique properties has been under intensive studies and many progresses have been achieved to separately understand them so far. However, as a unique case of the ferromagnetic–ferroelastic multiferroic material, whether and how the ferroelasticity and the ferromagnetism correlate with each other in $LaCoO_3$ films are not clear yet. Recent studies have observed structure domains in XRD and STEM experiments of $LaCoO_3$ thin films, which indicate correlation between ferromagnetism and ferroelasticity.[21,27,28] But the mechanism of the correlation has not been understood. On the other hand, recent progresses have extended the ferroelastic domains from the $LaCoO_3$ buffer layers to manganite oxides top layers.[29] Thus studies to purposely resolve possible correlations between the ferromagnetism and ferroelasticity are greatly demanded.

In this work, we fabricated $LaCoO_3$ thin films with thickness of 30 unit cells grown on TiO_2-terminated $SrTiO_3$ (001) substrates at different oxygen pressures. We found that the fine

[†]These authors contributed equally to this work.
[‡]Corresponding author. E-mail: chenglong1@shanghaitech.edu.cn
[§]Corresponding author. E-mail: zhaixf@shanghaitech.edu.cn

© 2024 Chinese Physical Society and IOP Publishing Ltd

tuning of the oxygen growth pressure tunes the stress and the elasticity in the $LaCoO_3$ films, evidenced by the controllable size of ferroelastic domains along both the [100] and [010] directions. More strikingly, it is found that films with larger (smaller) ferroelastic domains exhibit stronger (weaker) ferromagnetism. The synchrotron x-ray diffraction (XRD) studies reveal that films with stronger ferromagnetism and elastic force have substantially stretched octahedral backbones and significantly reduced octahedral rotations along the in-plane direction. Thus, the simultaneous appearance of ferroelasticity and ferromagnetism and their correlation can be explained by the elastic force tuning of the CoO_6 octahedral backbone structure. Therefore, this work reveals the mechanism of the correlated ferromagnetic and ferroelastic behaviors in the $LaCoO_3$ films mainly through the octahedral rotation, which potentially can be applied to develop new types of multifunctional materials based on the ferromagnetic and ferroelastic properties.

2. Methods

The $LaCoO_3$ thin films were grown with 0.1 Pa, 1 Pa, 15 Pa oxygen pressure using reflective high electron energy diffraction (RHEED) assisted pulsed laser deposition (PLD). The $SrTiO_3$ (001) substrates were etched with buffered hydrofluoric acid to have the TiO_2-terminated atomically-flat surface. The substrate temperature was 680 °C for all film growths. In the growth, the frequency of the excimer laser (248 nm wavelength) was 1 Hz and the laser energy density was about 1.5 J·cm^{-2}. The synchrotron XRD experiments were performed on the sector 33-BM beamline at Advanced Photon Source of Argonne National Laboratory. The x-ray beam size is 0.5 mm × 3 mm and the flux is ∼ 8 × 10^{11} photons·s^{-1}. The x-ray energy is 15.8 keV except for the energy scans at fixed diffraction position. The raw data were recorded using a pixel array detector (Pilatus 100k) at a distance of about 1 m from the sample.[30]

3. Results

The XRD ω–2θ scans of all the samples are shown in Fig. 1(a). Distinct Laue thickness fringes around the (002) Bragg peaks are observed, demonstrating the coherent epitaxy of $LaCoO_3$ films. The Bragg peak shift of different $LaCoO_3$ films indicates that the out-of-plane lattice constant increases with the reduced oxygen pressure during growth. The atomic force microscopy (AFM) image of the 15 Pa sample is also shown in Fig. 1(a) and AFM images of the other samples are shown in Fig. S1. The surfaces of all films are atomically flat with single-unit-cell height steps, similar to the surfaces of the substrates, which further confirm the high quality of all films. The magnetic properties of the $LaCoO_3$ films were characterized by the superconducting quantum interference device (SQUID). Figure 1(b) shows the in-plane M–T curves of all $LaCoO_3$ films, which were measured with a 0.1 T applied field after a 1 T field cooling. In this work, the in-plane direction denotes the (100) direction. The low temperature upturn originates from the superparamagnetism of the $SrTiO_3$ substrate.

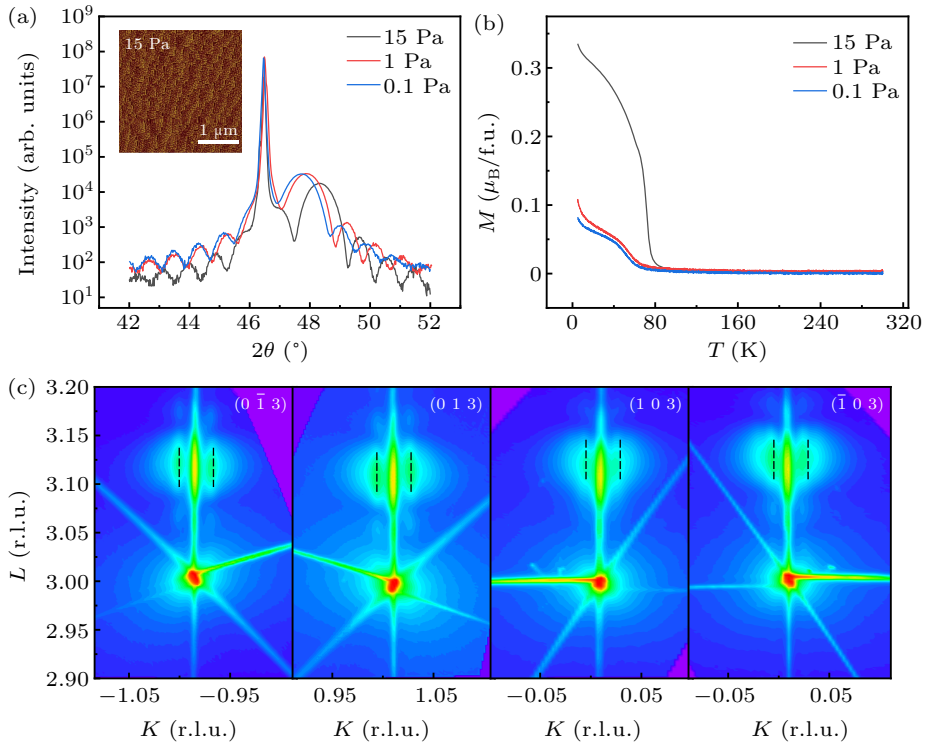


Fig. 1. Structural and magnetic characterizations for the $LaCoO_3$ films. (a) XRD ω–2θ scans of the $LaCoO_3$ films grown at different oxygen pressures. The inset shows the AFM image of the 15 Pa sample. (b) The M–T curves of all $LaCoO_3$ films. (c) The RSM data around {103} Bragg reflections of $SrTiO_3$ substrate for the 15 Pa sample. The dashed lines mark the positions of the satellite peaks along H and K directions.

The ferromagnetic transition temperatures (T_c) are 65 K, 70 K and 82 K for the 0.1 Pa, 1 Pa, and 15 Pa samples, respectively. The in-plane M–H curves of all films measured at the lowest temperature of 5 K are shown in Fig. S1(b), which reveal the larger saturation magnetization in films grown under higher oxygen pressure. Such observations are consistent with our previous work.[31]

In order to study the ferroelastic property of the $LaCoO_3$ films, we performed the three-dimensional (3D) reciprocal space map (RSM) measurements using the synchrotron XRD. Figure 1(c) shows the RSM data around {103} Bragg peaks of the $LaCoO_3$ film grown at 15 Pa oxygen pressure. The peak positions of the $LaCoO_3$ film along the H and K directions are the same as those of the $SrTiO_3$ substrates. It means that the $LaCoO_3$ film is coherently strained by the $SrTiO_3$ substrate. Since the lattice parameter of $SrTiO_3$ (3.905 Å) is larger than that of bulk $LaCoO_3$ (3.830 Å),[32] the $LaCoO_3$ film is under biaxial tensile strain. The c axis lattice of the $LaCoO_3$ film is thus compressively strained, which is measured to be 3.770 Å. More importantly, we find two satellite peaks appearing near the (103), ($\bar{1}$03), (013), (0$\bar{1}$3) Bragg reflections of the $LaCoO_3$ film along the H and K directions, as indicated by the dashed lines in Fig. 1(c). These satellite peaks are well known to be the fingerprint of the ferroelastic domains.[27,33] Different from the two-fold ferroelastic domains reported in the previous work,[27] we observe four-fold ferroelastic peaks along both the H and K directions. It indicates that the ferroelastic interaction in the current sample facilitates identical domain distributions along both the [100] and [010] directions (Fig. S2). From the distance of the satellite peaks in the reciprocal space, we can estimate the periodicity of the ferroelastic twin domains in the real space along the [100] and [010] directions. The twin domain periodicities are calculated to be 24.3 nm, 24.3 nm, 26.2 nm, 25.5 nm using satellite peaks nearest to the (103), ($\bar{1}$03), (013), (0$\bar{1}$3) Bragg reflections respectively, thus giving the average periodicity of about 25.1 nm in the $LaCoO_3$ thin films grown at 15 Pa oxygen pressure. Correspondingly, the size of the ferroelastic domains can be roughly estimated to be 12.5 nm (half of the periodicity), which is far below the size of the step width (about 230 nm).

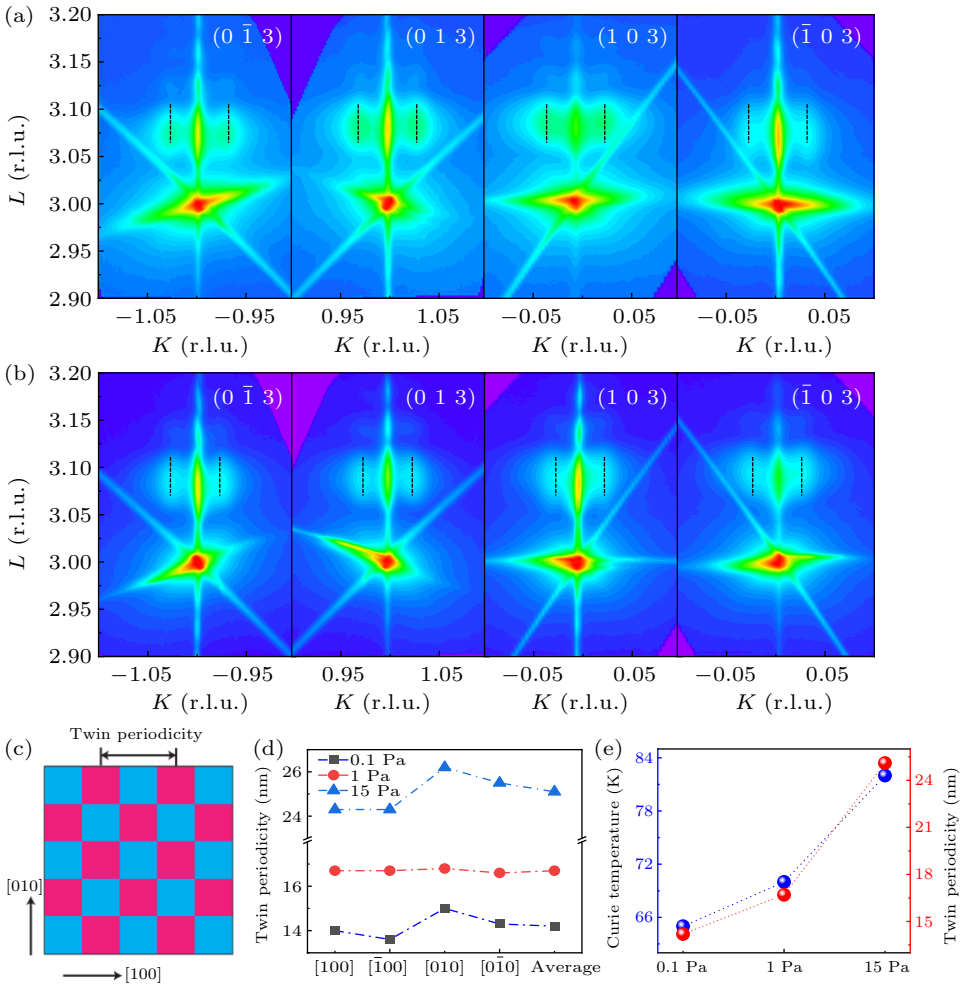


Fig. 2. The ferroelastic domains in the $LaCoO_3$ films. The RSM data around {103} Bragg reflections of $SrTiO_3$ substrate for the (a) 0.1 Pa and (b) 1 Pa samples. The dashed lines mark the positions of the satellite peaks along H and K directions. (c) The schematic illustration of the checkboard-type ferroelastic twin domains. (d) The periodicities of the ferroelastic twin domains at different directions in all $LaCoO_3$ films. The hollow signs represent the average value of the twin periodicities for each sample. (e) The dependence of ferromagnetic Curie temperature and twin periodicities on the growth pressure.

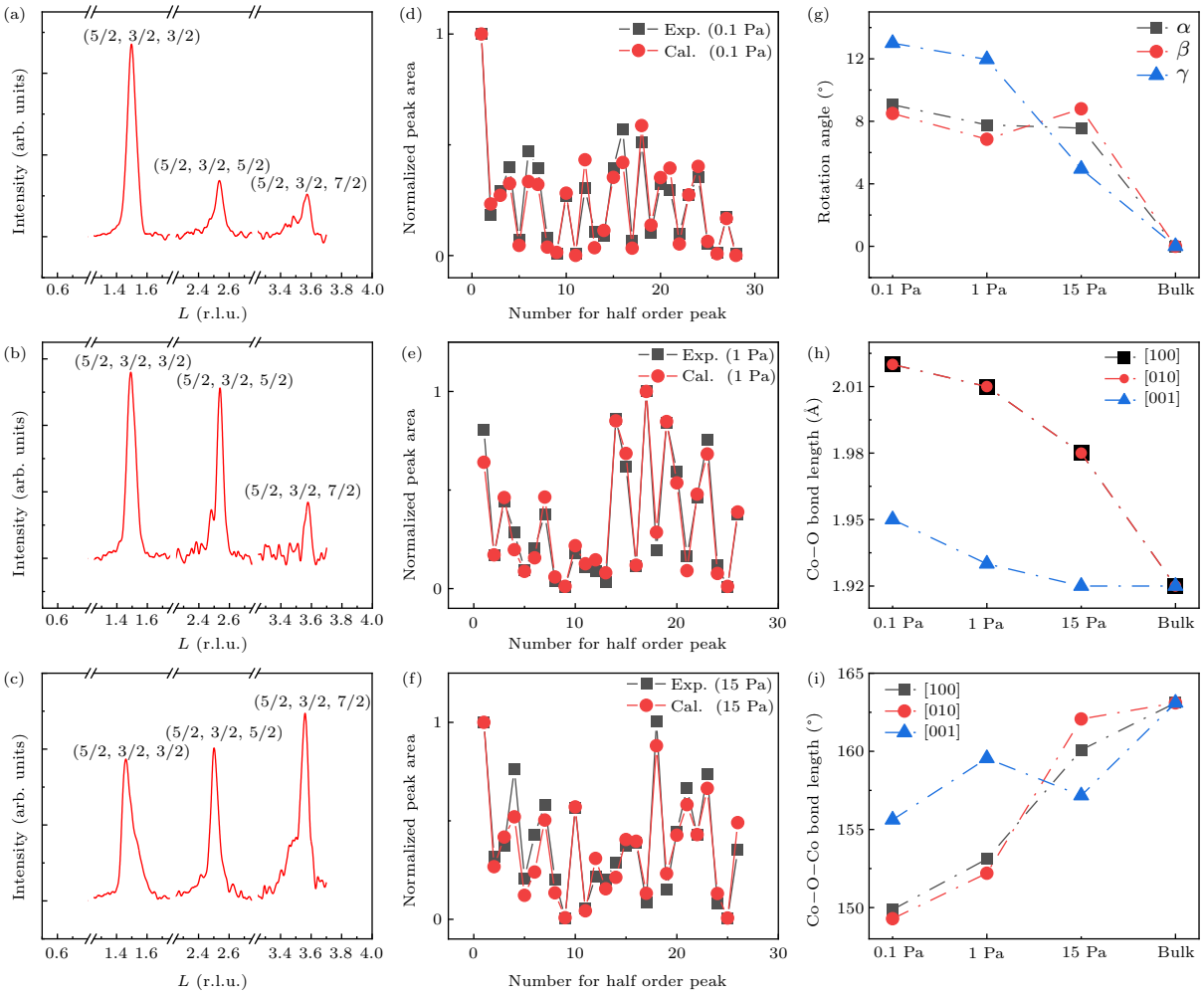


Fig. 3. Quantifications of the CoO_6 octahedra rotations. The half-order peaks (5/2, 3/2, *L*) of the (a) 0.1 Pa, (b) 1 Pa and (c) 15 Pa samples. (d)–(f) The fitting results of the half-order Bragg peaks. (g) The rotation angles along [100], [010] and [001] directions in the $LaCoO_3$ films. (h) The Co–O bong lengths along [100], [010] and [001] directions in the $LaCoO_3$ films. (i) The Co–O–Co bond angles along [100], [010] and [001] directions in the $LaCoO_3$ films.

Furthermore, we investigated the 3D RSMs of the other two films grown at 0.1 Pa and 1 Pa oxygen pressures for comparison. Figures 2(a) and 2(b) show the RSMs around the {103} Bragg peaks of the films and the $SrTiO_3$ substrates. Similar to the sample grown with 15 Pa oxygen pressure, the overlapping of the film peak and the substrate peak along the *H* and *K* directions reveals that the $LaCoO_3$ films grown with less oxygen environments are also coherently strained to the $SrTiO_3$ substrates. On the other hand, the film peak position along the *L* direction changes with the oxygen pressure. The *c* axis lattice constants of the $LaCoO_3$ films grown at 0.1 Pa and 1 Pa oxygen pressures are 3.811 Å and 3.797 Å, respectively. Both are larger than that of the film grown at 15 Pa oxygen pressure (3.770 Å). Nevertheless, satellite peaks also appear near the (103), ($\bar{1}$03), (013), (0$\bar{1}$3) Bragg reflections of the $LaCoO_3$ film along both *H* and *K* directions. Thus, similar checkboard-type ferroelastic domains also exist in the samples grown at lower oxygen pressures (Fig. 2(c)). However, the satellite-peak distances in the two samples grown at lower oxygen pressures differ significantly from that of the sample grown at 15 Pa oxygen pressure. Specifically, in the 1 (0.1) Pa sample, the periodicities of the ferroelastic twin domains are derived to be 16.7 (14.0) nm, 16.7 (13.6) nm, 16.8 (15.0) nm, and 16.6 (14.3) nm from satellite peaks nearest to the (103), ($\bar{1}$03), (013), (0$\bar{1}$3) Bragg reflections respectively. On average, the twin periodicities are 14.2 nm and 16.7 nm for the 0.1 Pa and 1 Pa samples, respectively, as shown in Fig. 2(d). One can notice that the periodicity of the ferroelastic twin domains systematically increases with the oxygen pressure applied during growth. Such a trend is identical to the ferromagnetism–oxygen pressure correlation as shown in Fig. 2(e). Therefore, a positive correlation between the strength of the ferromagnetism and the ferroelastic twin domain size is revealed.

In the perovskite structure, the flexible corner-shared octahedral network allows the epitaxial stress to be accommodated by either bond-length distortions, or by changes in the magnitude and phase of the octahedral rotations. If accommodated by the bond length change, usually the chemical valence change is the main solution of the structure change.[34] Otherwise, if the stress is mainly accommodated by the bond angle

change, the elastic force is mainly responsible for the structure change.[35] It is thus of significance to know whether the tensile stress exerted on the $LaCoO_3$ film stretches the Co–O bond length or straightens the bond angle. The rotation of the CoO_6 octahedral can be quantified by the analysis of half-integer peaks associated with the oxygen sub-lattice diffractions using the strong synchrotron light.[30] The octahedral rotations offset the oxygen atoms and double the unit cell, producing a distinctive set of half-order Bragg peaks depending on the tilt pattern. Figures 3(a)–3(c) show the typical half-order peaks with h, k, l indices all being half integers in all three films. Other measured half-order peaks are shown in supporting information. Peaks with one half integer or two half integer indices of h, k, l are not observed. Therefore, the octahedral rotation pattern is determined to be the rhombohedral type with out-of-phase rotations along all three directions. In the Glazer notation,[36] such rotation type is written as $a^-b^-c^-$, in which the $-$ sign indicates the out-of-phase rotation. The rotation angles around the a, b, and c axes (i.e., [100], [010] and [001] directions) are referred to be α, β, and γ, respectively.

In the following, we use all the measured half-order peak intensities to determine the octahedral rotation angles of α, β, and γ in all three films. Here the positions of the oxygen atoms are first individually calculated from the rotation matrix as described in previous works.[37,38] Then we calculate half-order Bragg peak intensities using the fitted positions of oxygen atoms. The calculated intensities are then fitted to the experimentally measured intensities, which gives us the rotation angles closest to the reality. The specific rotation angles determine the relative positions of all oxygen atoms. The calculation methods and details can be referred to the original works by May *et al.*[38,39] The accuracy of the fitting is demonstrated by the nice overlap of the fitted intensity and the measured intensity and very small residual errors, as shown in Figs. 3(d)–3(f). The rotation angles of the Co–O octahedra as functions of the sample growth pressure, together with those of the bulk $LaCoO_3$, are shown in Fig. 3(g). The α and β of all films do not have obvious trends of change as the growth pressure changes, which fluctuate between 7° and 9°. However, the γ clearly decreases with increasing oxygen pressure, and the decreasing trend is especially strong for the film grown at 15 Pa. Such a systematic trend of γ value change coincides with both the trends of the ferromagnetic transition temperature change and the ferroelastic domain size change.

The Co–O bond length along the three directions can be determined by the above rotation angles and the results are shown in Fig. 3(i). The Co–O bond length along [100] and [010] directions are almost the same and larger than that along the [001] direction. As the growth pressure increases, the bond length along the two in-plane directions systematically decreases and the decreasing trend is most significant for the 15 Pa sample. Moreover, the Co–O bond lengths along the [001] direction of films grown with 0.1 Pa and 1 Pa oxygen pressure are larger than that of bulk $LaCoO_3$. The [001]-direction Co–O bond length in the film grown with 15 Pa is slightly smaller than that of bulk $LaCoO_3$. Therefore, the bond length is shortened in films grown with high oxygen pressure, which weakens the possibility of Co valence change in accommodating the larger tensile stress in films grown at higher oxygen pressure. In Fig. 3(h), the Co–O–Co bond angles along both the in-plane and out-of-plane directions are shown, which reveals a straightening trend of the in-plane Co–O–Co zigzag chain in films of larger domain size. Thus, the scenario that octahedral backbone stretching accommodates the tensile stress is agreed.

4. Discussion

The most important finding in the current work is the strong dependence of both the twin domain and ferromagnetism on the oxygen growth pressure and the Co–O–Co bond angle in the film plane. In particular, the size of the ferroelastic domain and the transition temperature of the ferromagnetism both increase with the increasing oxygen pressure. According to the generalized Hooke's law,[40] we can correlate the stress along three directions as in the following equations:

$$\sigma_c = \varepsilon_c Y + \nu(\sigma_a + \sigma_b), \tag{1}$$

$$\sigma_a = \varepsilon_a Y + \nu(\sigma_c + \sigma_b), \tag{2}$$

where σ_a, σ_b and σ_c are the stresses exerted on the film along the [100], [010] and [001] directions, respectively. Y is the Young's modulus and ν is Poisson's ratio. ε_a and ε_c are the strains along the [100] and [001] directions, defined as $(a_{\text{film}} - a_{\text{bulk}})/a_{\text{bulk}}$ and $(c_{\text{film}} - c_{\text{bulk}})/c_{\text{bulk}}$, respectively.[41] Due to the cubic symmetry of the $SrTiO_3$ substrate, the strained $LaCoO_3$ film exhibits the tetragonal structure symmetry. Thus, σ_a and σ_b are the same and σ_c is equal to zero. Therefore equations (1) and (2) can be derived to be the following:

$$\sigma_a = -\frac{\varepsilon_c Y}{2\nu}, \tag{3}$$

$$\nu = \frac{\varepsilon_c}{\varepsilon_c - 2\varepsilon_a}. \tag{4}$$

As shown in the schematic diagram in Fig. 4(a), the two films grown with lower oxygen pressures of 0.1 Pa and 1 Pa are less compressed along the vertical direction, which have compressive strain of -0.496% and -0.862%, respectively. Comparatively, the film grown with 15 Pa exhibits a larger ε_c value of -1.566%. On the other hand, the in-plane strains of all three films are the same due to the coherent growth on $SrTiO_3$ substrates, i.e., $\varepsilon_a = 1.958\%$. Therefore, the Poisson's values of the three films are 0.112 (0.1 Pa), 0.180 (1 Pa), and 0.286

(15 Pa). Assuming a constant Young's modulus of 67 GPa,[42] the stress along a or b direction is 1.483 GPa, 1.604 GPa and 1.834 GPa for the three films respectively. That is, higher oxygen pressure during the growth generates stronger in-plane tensile stress in the $LaCoO_3$ film.

In order to understand the changes of the Poisson's ratio and the stress, the possible existence of oxygen vacancy has to be considered. At the low oxygen pressure, the $LaCoO_3$ film tends to incorporate more oxygen vacancies during the growth process. The oxygen vacancies release the tensile stress in the lateral lattice. Contrarily, the amount of oxygen vacancy is less in films grown with high oxygen pressure and the tensile stress in the lateral lattice is stronger, consistent with the above discussion. Moreover, the aggregation of oxygen vacancies is easier at the ferroelastic domain boundaries.[43] The schematic diagram of the domain boundary is show in Fig. 4(b). Based on our experimental finding, the size of the domain is larger (smaller) in films grown with high (low) oxygen pressure, and the domain assumes the square symmetry. By assuming that the oxygen vacancy surrounds square domain walls in Fig. 4(b), we calculate the number of oxygen vacancies in the edge of the squares. We can very roughly estimate the overall concentration of oxygen vacancies in the three $LaCoO_3$ films using the known size of the ferroelastic domain. The oxygen vacancy concentrations are approximately 0.92%, 0.78% and 0.52% for films grown at 0.1 Pa, 1 Pa and 15 Pa, respectively, which roughly agree to our previous work.[31] Thus, the $LaCoO_3$ film with fewer oxygen vacancies is more elastic evidenced by the larger ferroelastic domains.

The change of octahedral backbone structure can be understood in the following. In films grown at low oxygen pressures, the accommodation of the tensile stress is mainly through the Co–O bond elongation assisted by the oxygen vacancy. In films grown at high oxygen pressures, the accommodation of the tensile stress is through the in-plane Co–O–Co bond angle straightening compensated by the elastic energy. As results of the octahedral structure modulation, the magnetic properties of the $LaCoO_3$ films are greatly varied. As shown in Fig. 4(c), the crystal field energy gap (Δ_{cf}) exists between the threefold t_{2g} band and the twofold e_g band. The overall energy gap (Δ_E) between the t_{2g} and e_g bands is collectively controlled by Δ_{cf}, the exchange energy (Δ_{ex}) and the bandwidth (W) due to the strong hybridization between Co e_g orbital and the O 2p orbital. It can be expressed as $\Delta_E = \Delta_{cf} - \Delta_{ex} - W/2$. The crystal field energy Δ_{cf} is proportional to r_{Co-O}^{-5}, where r_{Co-O} is the Co–O bond length.[44] The bandwidth W is proportional to $r_{Co-O}^{-3.5}\sin(\theta/2)$, where θ is the Co–O–Co bond angle.[45] We assume that the Δ_{ex} is not affected by the modulation of the structure since it is an intrinsic material constant. Using the obtained average bond length and bond angle along a, b, c directions, we find Δ_{cf} varies little in films grown at different oxygen pressures whereas W is larger in films grown at higher oxygen pressures. Therefore, the overall energy gap Δ_E is smaller in films grown at higher oxygen pressures, which promotes spin up electrons occupying the e_g orbital and enhances the ferromagnetism.

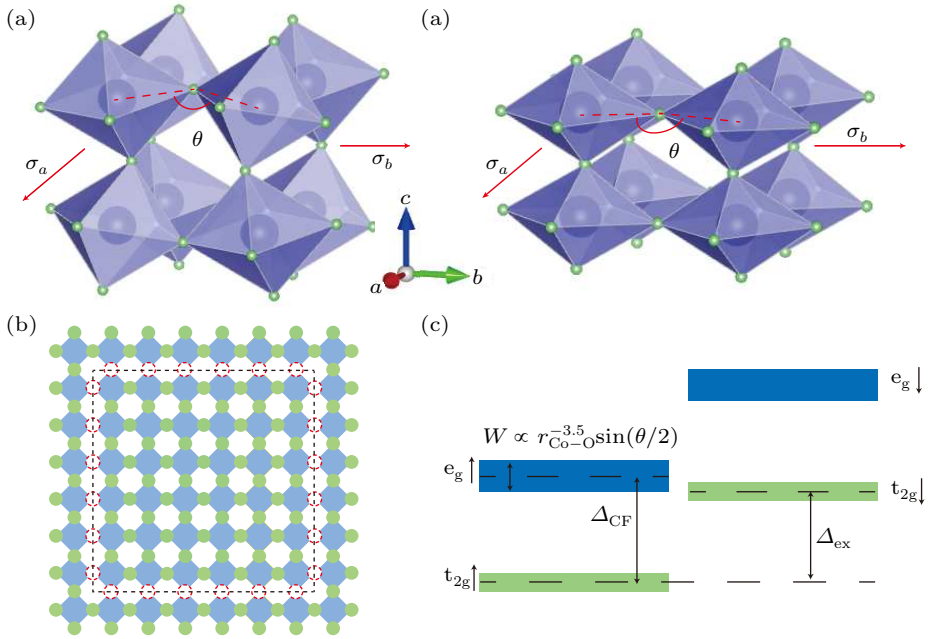


Fig. 4. The scenario of the ferroelastic–ferromagnetic coupling mediated by CoO_6 octahedral backbone stretching. (a) The illustration of the CoO_6 octahedral rotations under different tensile strains. The bolder arrows represent stronger strains. The dashed lines indicate the Co–O–Co bond angles. (b) The plane view of the ferroelastic domain with oxygen vacancy accumulation at the boundary. The green spots denote the oxygen atoms, the blue squares denote the CoO_6 octahedra. The dashed lines indicate the domain boundary where oxygen vacancies (red dashed circles) accumulate. (c) The schematic energy level diagrams of Co^{3+}. The $e_g\uparrow$, $t_{2g}\uparrow$ and $e_g\downarrow$, $t_{2g}\downarrow$ represent the spin-up and spin-down bands, respectively. W is the e_g orbital bandwidth. Δ_{cf} is the crystal field splitting. Δ_{ex} is the intra-atomic exchange energy.

5. Conclusion

In conclusion, we observed that the size of the ferroelastic twin domains and the ferromagnetic transition temperature are simultaneously enhanced or suppressed in tensile-strained $LaCoO_3$ films. The characterizations of the octahedral structure reveal that films with larger ferroelastic domains exhibit more straightened in-plane Co–O-Co bond angles. Furthermore, the straightened bond angle also broadens the Co 3d bandwidth which further decreases the energy gap Δ_E between t_{2g} and e_g, leading to the stronger ferromagnetism. Therefore, the Co–O octahedral backbone structure as the fundamental building block of the correlated oxides simultaneously controls the ferroelasticity and the ferromagnetism of the $LaCoO_3$ films grown with tensile strain. Such a study is very important for applications of magneto-mechanical coupled materials, and may pave the road for the rational design strategy of emergent multifunctional thin films.

Acknowledgments

Project supported by the National Natural Science Foundation of China (Grant Nos. 52072244 and 12104305), the Science and Technology Commission of Shanghai Municipality (Grant No. 21JC1405000), and the ShanghaiTech Startup Fund. This research used resources of the Advanced Photon Source, a U.S. Department of Energy (DOE) Office of Science User Facility operated for the DOE Office of Science by Argonne National Laboratory under Contract No. DE-AC02-06CH11357.

References

[1] Sun C, Alonso J A and Bian J 2021 *Adv. Energy Mater.* **11** 2000459
[2] Pan H, Li F, Liu Y, Zhang Q, Wang M, Lan S, Zheng Y, Ma J, Gu L, Shen Y, Yu P, Zhang S, Chen L Q, Lin Y H and Nan C W 2019 *Science* **365** 578
[3] Gu Z, Pandya S, Samanta A, Liu S, Xiao G, Meyers C J G, Damodaran A R, Barak H, Dasgupta A, Saremi S, Polemi A, Wu L, Podpirka A A, Will-Cole A, Hawley C J, Davies P K, York R A, Grinberg I, Martin L W and Spanier J E 2018 *Nature* **560** 622
[4] Yin Y W, Burton J D, Kim Y M, Borisevich A Y, Pennycook S J, Yang S M, Noh T W, Gruverman A, Li X G, Tsymbal E Y and Li Q 2013 *Nat. Mater.* **12** 397
[5] Mou X, Tang J, Lyu Y, Zhang Q, Yang S, Xu F, Liu W, Xu M, Zhou Y, Sun W, Zhong Y, Gao B, Yu P, Qian H and Wu H 2021 *Sci. Adv.* **7** eabh0648
[6] Izyumskaya N, Alivov Y and Morkoç H 2009 *Crit. Rev. Solid State Mater. Sci.* **34** 89
[7] Lu H, Bark C W, Esque D, Alcala J, Eom C B, Catalan G and Gruverman A 2012 *Science* **336** 59
[8] Lu X, Chen Z, Cao Y, Tang Y, Xu R, Saremi S, Zhang Z, You L, Dong Y, Das S, Zhang H, Zheng L, Wu H, Lv W, Xie G, Liu X, Li J, Chen L, Chen L Q, Cao W and Martin L W 2019 *Nat. Commun.* **10** 3951
[9] Li Q, Wang B, He Q, Yu P, Chen L Q, Kalinin S V and Li J F 2021 *Nano Lett.* **21** 445
[10] Lee D, Yoon A, Jang S Y, Yoon J G, Chung J S, Kim M, Scott J F and Noh T W 2011 *Phys. Rev. Lett.* **107** 057602
[11] Jaime M, Saul A, Salamon M, Zapf V S, Harrison N, Durakiewicz T, Lashley J C, Andersson D A, Stanek C R, Smith J L and Gofryk K 2017 *Nat. Commun.* **8** 99
[12] Bozorth R M, Tilden E F and Williams A J 1955 *Phys. Rev.* **99** 1788
[13] Hong S S, Gu M, Verma M, Harbola V, Wang B Y, Lu D, Vailionis A, Hikita Y, Pentcheva R, Rondinelli J M and Hwang H Y 2020 *Science* **368** 7
[14] Huang J, Wang H, Sun X, Zhang X and Wang H 2018 *ACS Appl. Mater. Interfaces* **10** 42698
[15] Balke N, Choudhury S, Jesse S, Huijben M, Chu Y H, Baddorf A P, Chen L Q, Ramesh R and KalininS V 2009 *Nat. Nanotechnol.* **4** 868
[16] Chai Y S, Cong J Z, He J C, Su D, Ding X X, Singleton J, Zapf V and Sun Y 2021 *Phys. Rev. B* **103** 174433
[17] Zheng H, Wang J, Lofland S E, Ma Z, Mohaddes-Ardabili L, Zhao T, Salamanca-Riba L, Shinde S R, Ogale S B, Bai F, Viehland D, Jia Y, Schlom D G, Wuttig M, Roytburd A and Ramesh R 2004 *Science* **303** 661
[18] Hoch M J R, Nellutla S, Tol v J, Choi E S, Lu J, Zheng H and Mitchell J F 2009 *Phys. Rev. B* **79** 214421
[19] Freeland J W, Ma J X and Shi J 2008 *Appl. Phys. Lett.* **93** 212501
[20] Fuchs D, Pinta C, Schwarz T, Schweiss P, Nagel P, Schuppler S, Schneider R, Merz M, Roth G and Löhneysen H V 2007 *Phys. Rev. B* **75** 144402
[21] Yoon S, Gao X, Ok J M, Liao Z, Han M G, Zhu Y, Ganesh P, Chisholm M F, Choi W S and Lee H N 2021 *Nano Lett.* **21** 4006
[22] Choi W S, Kwon J H, Jeen H, Hamann-Borrero J E, Radi A, Macke S, Sutarto R, He F, Sawatzky G A, Hinkov V, Kim M and Lee H N 2012 *Nano Lett.* **12** 4966
[23] Guo E J, Desautels R, Lee D, Roldan M A, Liao Z, Charlton T, Ambaye H, Molaison J, Boehler R, Keavney D, Herklotz A, Ward T Z, Lee H N and Fitzsimmons M R 2019 *Phys. Rev. Lett.* **122** 187202
[24] Feng Q, Meng D, Zhou H, Liang G, Cui Z, Huang H, Wang J, Guo J, Ma C, Zhai X, Lu Q and Lu Y 2019 *Phys. Rev. Mater.* **3** 074406
[25] An Q, Xu Z, Wang Z, Meng M, Guan M, Meng S, Zhu X, Guo H, Yang F and Guo J 2021 *Appl. Phys. Lett.* **118** 081602
[26] Fuchs D, Dieterle L, Arac E, Eder R, Adelmann P, Eyert V, Kopp T, Schneider R, Gerthsen D and Löhneysen H V 2009 *Phys. Rev. B* **79** 024424
[27] Guo E J, Desautels R, Keavney D, Roldan M A, Kirby B J, Lee D, Liao Z, Charlton T, Herklotz A, Ward T Z, Fitzsimmons M R and Lee H N 2019 *Sci. Adv.* **5** eaav5050
[28] Chaturvedi V, Walter J, Paul A, Grutter A, Kirby B, Jeong J S, Zhou H, Zhang Z, Yu B, Greven M, Mkhoyan K A, Birol T and Leighton C 2020 *Phys. Rev. Materials* **4** 034403
[29] Ji Y, Chen P, Zhu M, Liu J, Gao X, Li L, Wang L, Bai X, Chen K and Liao Z 2023 *Appl. Phys. Lett.* **122** 072901
[30] Zhai X, Cheng L, Liu Y, Schlepütz C M, Dong S, Li H, Zhang X, Chu S, Zheng L, Zhang J, Zhao A, Hong H, Bhattacharya A, Eckstein J N and Zeng C 2014 *Nat. Commun.* **5** 4283
[31] Meng D, Guo H, Cui Z, Ma C, Zhao J, Lu J, Xu H, Wang Z, Hu X, Fu Z, Peng R, Guo J, Zhai X, Brown G J, Knize R and Lu Y 2018 *Proc. Natl. Acad. Sci. USA* **115** 2873
[32] Sterbinsky G E, Ryan P J, Kim J W, Karapetrova E, Ma J X, Shi J and Woicik J C 2012 *Phys. Rev. B* **85** 020403
[33] Salje E K H 2012 *Annu. Rev. Mater. Res.* **42** 265
[34] Brown I D, Dabkowski A and McCleary A 1997 *Acta Cryst.* **B53** 750
[35] Woodward P M 1997 *Acta Cryst.* **B53** 44
[36] Glazer A M 1972 *Acta Cryst.* **B28** 3384
[37] Cao H, Guo H, Shao Y C, Liu Q, Feng X, Lu Q, Wang Z, Zhao A, Fujimori A, Chuang Y D, Zhou H and Zhai X 2021 *Nano Lett.* **21** 3981
[38] May S J, Kim J W, Rondinelli J M, Karapetrova E, Spaldin N A, Bhattacharya A and Ryan P J 2010 *Phys. Rev. B* **82** 014110
[39] May S J, Smith C R, Kim J W, Karapetrova E, Bhattacharya A and Ryan P J 2010 *Phys. Rev. B* **82** 014110
[40] Lempriere B M 1968 *AIAA Journal* **6** 2226
[41] Chen S, Guan C, Ke S, Zeng X, Huang C, Hu S, Yen F, Huang H, Lu Y and Chen L 2018 *ACS Appl. Mater. Interfaces* **10** 18029
[42] Lugovy M, Verbylo D, Orlovskaya N, Reece M, Kuebler J, Graule T and Blugan G 2021 *Materials* **14** 3543
[43] Dawber M and Scott J F 2000 *Appl. Phys. Lett.* **76** 1060
[44] Qiao L, Jang J H, Singh D J, Gai Z, Xiao H, Mehta A, Vasudevan R K, Tselev A, Feng Z, Zhou H, Li S, Prellier W, Zu X, Liu Z, Borisevich A, Baddorf A P and Biegalski M D 2015 *Nano Lett.* **15** 4677
[45] Zhou J S, Yan J Q and Goodenough J B 2005 *Phys. Rev. B* **71** 220103